USSR ACADEMY OF SCIENCES
A.F. IOFFE ORDER OF LENIN PHYSICO-TECHNICAL INSTITUTE, LENINGRAD
Report 429

METHOD FOR MEASURING THE HADRON-PROTON SCATTERING CROSS-SECTION IN THE COULOMB INTERFERENCE REGION

A.A. Vorob'ev, Yu.S. Grigor'ev, A.S. Denisov, Yu.K. Zalite,
G.A. Korolev, V.A. Korolev, G.G. Kovshevnyj, N.K. Lastochkin,
E.M. Maev, V.I. Medvedev, G.L. Sokolov, G.E. Solyakin,
E.M. Spiridenkov, I.I. Tkach and V.A. Shchegel'skij

Leningrad 1972

Translated at CERN by R. Luther
(Original: Russian)
Not revised by the Translation Service

(CERN Trans. Int. 73-2)

Geneva
February 1973

Sent to: "Nucl. Instr. and Meth."

A parallel-plate ionization chamber with a grid filled with hydrogen is used to measure the differential cross-sections of elastic hadron-proton scattering at small angles. The chamber serves both as a gas target and as a detector of recoil protons. By measuring the shape of the signals on the chamber's electrodes and the signals' delay time in relation to the instant when a scattered particle passes through the chamber, the recoil proton's energy and emission angle may be determined and the gas target's volume defined inside the chamber's useful volume. The energy range of the recoil protons is 1.0 - 4.0 MeV. The energy resolution is 40 keV. The method is applied over a wide energy range with intensities of 10^4 - 10^5 particles/second.

By measuring the differential cross-section of elastic hadron scattering in the Coulomb and nuclear interference regions, the real part of the spin-independent forward scattering amplitude (Re $A_{ns}(0)$) may be determined. This value may also be calculated from dispersion relations. The latter may thus be checked, hence the interest in this problem.

The momentum transfer region /t/ in which there is considerable interference is determined by the Coulomb A_c and nuclear amplitude equation

$$A_c(t) \simeq \mathrm{Im}\, A_{ns}(0) \equiv \frac{k}{4\pi} \cdot \sigma_{tot}$$

$$A_c(t) \simeq \frac{2}{137} \frac{k}{|t| \beta_p}$$

Here $|t| \simeq \frac{0.1}{\sigma_{tot.}\ (\mathrm{mbarn})}$, and β_p is the velocity of the incident particle. The total cross-section $\sigma_{tot.}$ depends slightly on the energy of the scattered particle and at high energies is 40-25 mbarn when protons, $\pi^{\pm}$ or $K^{\pm}$ are scattered on protons. It therefore depends slightly on the energy and type of particle, and the region of /t/ values in which the interference experiment (Fig. 1) must

be performed is:

$$2.10^{-3} < /t/ < 10^{-2} (GeV/c)^2.$$

The experimental value of /t/ may be defined either by measuring the scattering angle of the primary particle: $/t/ \approx p^2 \Theta^2$, or by measuring the kinetic energy of the recoil proton T_p: $/t/ = 2MT_p$. Use is made of both these possibilities at present. A typical layout of an experiment to measure the angle Θ of the scattered particle is shown in Fig. 2. The particle beam is shaped by means of a system of lenses, collimators and bending magnets. A hydrogen target is used as the scatterer. The particle's angle of incidence on the target and its emission angle are determined by means of a set of spark chambers S_1, S_2, S_3, S_4. The momentum of the scattered particles is analyzed by means of a magnet and spark chambers S_5. A momentum analysis is essential in order to separate elastic from inelastic events. Different versions of this device have been developed in various laboratories, especially at CERN /1/, Brookhaven /2/ and Dubna /3/. One definite advantage of the system is the high recording efficiency which makes it possible to use low-intensity beams, including secondary particle beams. The scattering of protons, $\pi^{\pm}$ mesons and antiprotons on protons was investigated in the energy range up to 20 GeV. It is also possible in principle to study K^-p scattering. One disadvantage of this method for detecting the scattered particle, apart from its complexity, is that it is difficult to allow for systematic errors. Consequently, the data obtained, for instance, by the Lindenbaum group from the measurement of the real part of the π^- meson scattering amplitude have changed over the years. Moreover, there is a discrepancy between the results obtained by the CERN and Brookhaven groups who investigated pp scattering at E_p = 20 GeV. As the energy of the scattered particles increases, it becomes more and more difficult to measure small angles and identify elastic events.

In recent years, the recoil nuclei technique /4/ has been developed and successfully used at Dubna in order to analyze pp scattering. An internal target has been used as the scatterer (a thin film containing hydrogen or a gas jet) in order to ensure the multiple

($\sim 10^5$) traversal of accelerated protons. The energy of the recoil protons was measured in terms of their path in photoemulsion chambers and later by means of semiconductor detectors. The recoil proton's angle of emission was also measured in order to deduct the background of inelastic events. As the energy range of the recoil protons in the interference region is virtually independent of the energy of the scattered particles, the technique of recoil nuclei may be used over a wide energy range. The method is simple and ensures a sufficiently high accuracy for the measurement of $d\sigma/dt$ and yet it may be used only to study pp scattering as it requires an exceptionally high primary beam intensity. The method's low recording efficiency is due, firstly, to the thinness of the target and, secondly, to the detector's small solid angle.

This report describes a method for measuring the parameters of recoil protons in the interval $2.10^{-3} \leqslant |t| \leqslant 8.10^{-3}$ (GeV/c)^2 by means of a pulsed ionization chamber which is filled with hydrogen, which possesses a much higher recording efficiency and which can operate with low-intensity beams (10^4 - 10^5 particles/sec.) of various particles (π , K, d, n, $\bar{p}$) over a wide scattered particle energy range. The parameters of the scattered particle may be measured at the same time as the parameters of the recoil proton so that it is relatively easy to separate out background reactions when studying high-energy particle scattering.

DESCRIPTION OF THE METHOD FOR RECORDING RECOIL PROTONS

The method is based on the use of a pulsed ionization chamber filled with hydrogen which serves both as a gas target and as a detector of recoil protons. The chamber enables the physicist to determine the energy and emission angle of the recoil proton and also the position of the track inside the chamber's useful volume. The chamber is of the parallel-plated type and includes a grid in which the cathode and anode consist of a central and an orifice electrode (Fig. 3). The scattered particles traverse the chamber close to its axis and perpendicular to the surface of the electrodes.

Recoil protons occuring in the volume between the cathode and the grid are recorded. Recoil protons corresponding to elastic scattering at small angles are almost parallel to the surface of the electrodes. The pressure of the gas in the chamber and the dimensions of the electrodes are selected so that the path of recoil protons with an energy of up to ~ 5.0 MeV fits into the chamber's sensitive volume, which is defined by the external diameter of the orifice electrodes. As it slows down, the proton ionizes the gas in the chamber, forming electron-ion pairs and the number of ion pairs is proportional to the energy Tp. The electric field causes the electrons to drift towards the grid, pass through it and collect on the anode. Pulses then occur at the central cathode (from now on "cathode"), central anode ("anode") and orifice anode ("orifice"). These pulses are shown schematically in Fig. 4.

By measuring the pulse height at the anode (or the sum of the pulse heights at the anode and orifice if the proton's path is greater than the anode's radius), the energy of the recoil proton Tp may be determined. The recoil proton's emission angle φ in relation to the chamber axis is determined according to the value of the leading edge t_f of the pulse at the anode. Elastic events correspond to pulses with a minimal t_f value. By measuring the time interval $t_a - t_o$, it is possible to determine the distance from the grid to the nearest end of the track. Additional information on the position of the track inside the chamber volume is provided by the pulse height from the cathode V_c. This pulse is used to calibrate the scale $t_a - t_o$. By defining the angle φ and the value $t_a - t_o$, particles occuring in the electrodes (or behind the electrodes) and remaining within the chamber's useful volume may be excluded from the recording. However, useful events with an interaction point in the immediate vicinity (~ 10 mm) of the cathode and grid must also be excluded. In other words, the gas target's volume is less than the volume delineated by the cathode and grid and the error in defining the thickness of the target is the limit to accuracy in absolute measurements of the value $d\sigma/dt$ using this method. It will be shown below that this error may be reduced to 1-2%.

A major problem is the elimination of background reactions occuring inside the gas target. These reactions include, first and foremost, elastic scattering with large momentum transfer when the path of the recoil proton does not fit into the chamber's useful volume. These events are eliminated by correlating the pulses from the anode and orifice. Background reactions also include inelastic scattering accompanied by the production of mesons. The emission angle of the recoil proton is used to identify these events. The number of particles passing through the chamber is determined by a direct count by a telescope of scintillation counters S_1 S_2 S_3 operating in coincidence with the pulse V_c. This mode of chamber control considerably reduces the background of nuclear reactions and the background caused by the scattering of neutrons in the chamber's sensitive volume. An even more efficient means of excluding background reactions would be the use of a trigger system of proportional chambers, to be described below.

Each primary particle passing through the chamber leaves approximately 40 keV in the sensitive volume. (Ions produced in the space between the cathode-guard electrode and anode-guard electrode recombine).

Consequently, pulses occur at the cathode and anode, and the chamber's energy resolution may deteriorate. This effect is reduced by means of a compensator which is triggered from scintillation counters S_1 . S_2 whenever a charged particle passes through, and which carries pulses similar in shape to those occuring at the cathode and anode but opposite in sign. By combining the pulses, the effect of the beam on the chamber's resolving power may be considerably reduced. Beams of up to 10^5 particles/sec. may be used.

The data acquisition rate when using a chamber with the parameters shown in Fig. 3 at $\sigma_{tot.}$ = 40 mb and at an intensity of 10^4 particles/sec. is approximately 120 useful events per hour in the range 1 MeV $\leq T_p \leq$ 4.0 MeV.

GAS PURITY. RECOMBINATION AND ADHESION OF ELECTRONS

The presence of electronegative admixtures in the useful gas of an ionization chamber with electron connection leads to the loss of electrons which collect on the anode due to adhesion. Consequently, the energy resolution deteriorates and the energy line is shifted. The main electronegative admixture is oxygen. The cross-section for the adhesion of electrons to oxygen is at a minimum at a mean electron energy of 0.8 - 1.5 eV. Therefore, the usual method for reducing adhesion (apart from gas purity) is either to select an appropriate $\mathcal{E}/p$ ratio ($\mathcal{E}$ - electric field intensity, p - pressure) or to add a certain amount of multi-atomic gas in order to obtain an optimum value for the mean electron energy /5/. However, when the hydrogen is at several atm., several hundreds of kilovolts would have to be applied to the chamber electrodes in order to achieve the optimum mean electron energy. This is due to the fact that the H_2 molecule has low excitation levels and the electrons effectively lose energy in inelastic collisions. Therefore, there is only one solution: carefully to outgas the chamber and clean the used hydrogen.

Mention has also been made in previous papers of the difficulty of achieving a saturation voltage, i.e. a voltage at which the recombination of ions ceases to have a significant effect. However, as will be shown below, it is again a question of gas purity. The co-efficient of electron-ion recombination in hydrogen seems to be sufficiently low (approximately the same as in argon), but the adhesion of the electrons in fact leads to ion-ion recombination, the probability of which is approximately 10^4 times greater.

The above considerations were taken into account when designing the chamber. The chamber body was made from stainless steel. The inner surface was electro-polished and chemically cleaned. The lining was made from copper and indium. Lengthy vacuum training with heating was carried out. As a result, in-leakage into the chamber did not exceed 10^{-3}mm Hg per 24 hours. The hydrogen used to fill the ionization chamber was purified by a cryogenic method. The

electrolytic hydrogen passed through a drying unit, a low-temperature cleaning unit cooled by liquid nitrogen, and a palladium catalyst. The hydrogen's degree of purity after it has passed through all the units was checked by GL 5108 gas analyzers which determined the oxygen content. The hydrogen was liquefied if the oxygen content did not exceed 10^{-3}%. Part of the liquefied hydrogen from the Dewar flask was evaporated into an intermediate store which had been previously evacuated and scrubbed with pure hydrogen. The evaporating hydrogen was then pumped by a diaphragm compressor MK 2.5/200 into standard hydrogen cylinders. The amount of impurities in each cylinder was estimated by means of a "Tsvet-4" chromatograph with a thermal conduction detector. As the threshold sensitivity of the detector was inadequate, the usual method of cleaning at a liquid nitrogen temperature was used. The following data were obtained:
Content $N_2 \leq (3\text{-}6)\cdot 10^{-3}$%, $O_2 + Ag \leq 4\cdot 10^{-4}$% per volume.

Figure 5 shows the dependence of the ^{234}U α-particle pulse heights (source placed at the cathode) on the voltage at the cathode. The curve virtually reaches saturation at 9 kV. A flat top is a definite guarantee of the absence of recombination and adhesion, and this may be confirmed by a comparison with the curve obtained 125 hours after filling. By this time the total amount of impurities in the gas was $\leq 10^{-6}$ due to in-leakage. The amount of electronegative impurities in the original gas does not seem to be more than 10^{-7}. Proof of the absence of adhesion and recombination was obtained in an experiment in which the pulse of the α-particles was measured at various gas pressures in the chamber - 8 atm., 4 atm. and 2 atm. at the same δ/p ratio. In this case the adhesion effect must have decreased linearly with pressure (the recombination effect decreased even more rapidly). However, no variation in pulse height was observed ($\leq$ 0.5%). Lastly, the absence of adhesion was confirmed in the same experiment by measuring pp scattering. Fig. 6 shows the height distribution peaks for pulses at the anode representing recoil protons, at fixed pulse heights at the orifice, (the energy of the recoil protons is determined in this way). The distributions shown correspond to recoil protons produced in various parts of the chamber. When there

is adhesion, the points for the area closest to the cathode would have to be lower. However, no shift is observed. In fact, where there is absolutely no adhesion, there must be a shift to the opposite side as the grid is not shielded. In this case, the lack of shielding is compensated by the adhesion effect. Calculations show that the adhesion effect observed is due entirely to in-leakage (measurements carried out 72 hours after filling). There is virtually no adhesion ($\leq 0.5\%$) in the original gas. Therefore, some "contamination" of the gas is even useful as it makes up for the effect due to the lack of shielding.

Consequently, 1) when using sufficiently pure hydrogen containing $\leq 10^{-7}$ electronegative impurities, recombination and adhesion may be eliminated, 2) in its present design, the chamber may be operated for a few days without refilling.

ELECTRON MOBILITY AND DIFFUSION

Fig. 7 shows the dependence on $\mathcal{E}/p$ of the electron's rate of drift in hydrogen. The drift rate determines the chamber's time characteristics - the resolving time and also the accuracy with which angle φ is measured. As shown in Fig. 7, electron mobility in hydrogen is not great. Under operating conditions the electron drift times from cathode to grid and from grid to anode are 17/usec and 2/usec respectively (Fig. 8). Electron diffusion during collection in the chamber may lead to a distortion of the leading edge of the pulse at the anode and consequently to a deterioration of the accuracy with which angle φ is measured. Blurring of the track due to diffusion may be estimated by the following formula

$$\sigma(t_a) = \sqrt{2 \cdot D (t_a - t_o)} ,$$

$$D = \frac{1}{3} \cdot \frac{L}{p} \cdot u ,$$

where σ (ta) - standard deviation of electrons on track centre,

D - electron diffusion co-efficient in hydrogen,

$t_a - t_o$ - electron drift time across grid-cathode gap,

L - length of electron's free flight in hydrogen at 1 mm Hg,

P - pressure of hydrogen in chamber,

U - mean velocity of electrons.

By applying the values $U = 2 \cdot 10^7$ cm/sec, $L = 3.6 \cdot 10^{-2}$ cm /6/, corresponding to a useful field in the chamber of $\mathcal{E}/p = 0.2$ V/cm·mm Hg we obtain $\sigma = 0.3$ mm for a maximum drift time of 17/usec. Therefore, the blurring of the tracks is comparatively small. This is confirmed by photographs of a pulse generated by an α-particle emerging almost parallel to the surface of the cathode (Fig. 8b).

ENERGY RESOLUTION

The energy resolution of the ionization chamber is determined above all by the pre-amplifiers' noise level. Fig. 9 shows the dependence of the noise level produced by the pre-amplifiers on the value of the input capacitors and on the amplifiers' pass band. The capacitance of the central anode $C_a \simeq 40$ pF and $\tau_o = 20$/usec ($\tau_o = \tau_a = \tau_g$). The corresponding noise level is FWHM = 35 keV. The capacitance of the orifice anode $C_{oa} = 100$ pF, $\tau_o = 20$/usec and the noise FWHM = 50 keV. The capacitance of the cathode $C_c = 30$ pF, $\tau_o = 35$/usec and noise FWHM = 35 keV. These parameters were obtained under operating conditions and are not boundary values. They depend to a large extent on the quality of the field transistors used at the pre-amplifier input and on the degree of interference suppression. A considerably lower noise level of FWHM = 21 keV was achieved during tests on a dummy chamber (Fig. 10).

Fluctuation in the number of ion pairs ΔN at a fixed T_p value have also a certain effect on the energy resolution. However, this effect is not great. The standard fluctuation in the number of ion pairs ΔN is determined by the Fano formula /7/

$$\Delta N = \sqrt{F \cdot W \cdot T_p} \quad ,$$

where W is the mean energy factor for the production of ion pairs,
F is the Fano factor.

For hydrogen W = 36 eV, and F $\simeq$ 0.3. Hence, ΔN = 6 keV at T_p = 3 MeV.

The grid used in the chamber is not an ideal shield against the induction effect of positive ions. Therefore, the real pulse at the anode is reduced:

$$V_a = \frac{T_p}{W.C_a}\left(1 - \delta\,\frac{\bar{x}}{d}\right),$$

where δ is the grid's transmission co-efficient,
$\bar{x}$ is the distance from the track's centre of gravity to the cathode,
d is the grid-cathode distance.

For the given design δ = 0.018 /8/. (The distance between the wires is 1.5 mm, the diameter of the wires is 0.1 mm and the grid-anode distance is 20 mm). Therefore the pulse height V_a may vary by 1.8% depending on the position of the track in the chamber. However, as the position of the track is known, then appropriate corrections may be introduced when processing the results. Therefore, the transmission of the grid does not have an adverse effect on the energy resolution.

The pulse height V_a may also be reduced due to adhesion of electrons. Let η be the proportion of electrons lost during drift from the cathode to the grid. Then

$$V_a = -\frac{T_p}{WC_a}\left(1 - \eta + \eta\,\frac{\bar{x}}{d}\right).$$

If we take into account the simultaneous effect of grid transmission and electron adhesion, then

$$V_a = -\frac{T_p}{WC_a}\left[1 - \eta - (\delta - \eta)\,\frac{\bar{x}}{d}\right].$$

At $\eta = \delta$ the two effects are fully compensated and

$$V_a = - \frac{T_p}{WC_a} (1 - \eta).$$

The actual situation is quite similar to this (viz. Fig. 6).

Pulses occuring at the chamber electrodes due to the ionization of the sensitive volume by primary particles also lead to deterioration in the resolving power. The amplitude of these signals may be 20-40 keV depending on the τ_o value, and two or more pulses may be superimposed when there is a loading of 10^4 particles/sec. In order to reduce the effect of beam on energy resolution, use is sometimes made of compensation chambers, i.e. chambers through which the beam passes, and the pulses thus generated are deducted from the pulses generated in the main chamber. However, in this case there is a build-up of amplifier noise. For this experiment, a "noise-free" compensator circuit is used which is triggered by pulses from scintillation counters S_1 ^ S_2 and which emits signals completely equivalent to the signals from the ionization chamber. This same circuit may emit a prohibit signal when there is a surge in beam intensity. When using the compensator with a beam of $2 \cdot 10^4$ protons/sec., there was no increase in the width of the α-line and generator line. It seems that satisfactory resolution may also be obtained at 10^5 protons/sec.

Consequently the chamber's energy resolution is approximately 40 keV in the range 1 - 3 MeV and approximately 70 keV in the range 3 - 4 MeV when the sum of the pulses from the anode and the orifice are used in order to measure the energy.

ENERGY CALIBRATION

The energy calibration of the V_a and V_{oa} pulses was found by using ^{234}U sources ($E\alpha$ = 4.76 MeV) as reference points. The linear dependence of the pulse height on the recoil proton energy was thus obtained. However, this dependence was not determined

experimentally. Moreover, there is no accurate information available at present to indicate whether the energy used to produce ion-electron pairs in hydrogen is the same for α-particles and for protons /9/.

Therefore, additional calibration measurements had to be carried out in order to measure the recoil proton energy by the ionization method. The calibration was done by analyzing directly elastic events recorded during experiments to investigate pp scattering. The energy of the recoil protons was determined according to their path. The dependence of the proton energy on the path in hydrogen is known with sufficient accuracy /10/ ($\sim$ 1%). The calibration was done in the following way. Pulses from the anode and orifice were used. Using the data from report /10/, plots were made of the dependences of the energy left by the protons at the anode and orifice on the total proton energy (Fig. 11). Fig. 12 shows the matrix of events in the co-ordinates anode pulse height-orifice pulse height which was obtained by experiment. The event distribution has a characteristic triangular form. For track lengths not exceeding the anode radius, the pulse height at the orifice is close to zero (induced pulses). Events with track lengths greater than the anode radius but less than the outside radius of the orifice form the topside of the triangle. They correspond to increasing V_{oa} and vanishing V_a. Lastly, the third side of the triangle, - vanishing V_a and V_{oa} -, represents events for which the particle track exceeds the outside radius of the orifice. For a given V_{oa} pulse height, the anode pulse height spread is mainly determined by the spreading of the beam in relation to the centre of the chamber and, to a lesser extent, by the energy resolution. By applying this dependence, it is possible to reconstruct the beam profile averaged in terms of the azimuthal angle (Fig. 13); this profile is in good agreement with direct measurements on the beam. When plotting this curve, the recoil proton energy $T_p = V_a + V_{oa}$ and its total path $R_{tot.}$ were first found, and then the value $R_{tot.}$ was used to calculate the value R_{oa} which corresponds to the energy V_{oa}. The energy scale V_a and V_{oa} was determined by linear calibration in terms of α -particles. When summing the pulse heights from the anode and orifice, mutual induction must be taken into account. This value depends on the ratio of the

mutual capacitance between the anode and orifice to the capacitance of the anode or orifice in relation to earth. In order to reduce the induced pulses, pre-amplifiers with a high capacitive feed-back were connected to the anode and orifice. As a result the induction value totals approximately 1.4% of the pulse height.

The position of the peak of the reconstructed beam profile coincided accurately with the anode radius (more accurately with the distance from the anode centre to the middle of the anode-orifice gap). Similar curves were plotted for various incident proton beam energies; 1000 MeV, 750 MeV, 700 MeV, 650 MeV and 510 MeV. In all cases the position of the peak equals the anode radius, from which it may be concluded that the linear calibration is acceptable and $W_\alpha / W_p = 1$. The accuracy of this calculation is $\sim 3\%$, taking into account possible errors in the path-energy dependence and in the measurements.

ANGULAR RESOLUTION

The angle of the recoil proton is defined in terms of the leading edge t_f of the pulse at the anode:

$$t_f = t_{f\ min.} + \frac{Z}{W}$$

where Z is the projection of the track to the chamber axis,

W is the electron's drift rate in the cathode-grid volume,

$t_{f\ min.}$ corresponds to tracks parallel to the surface of the electrodes and is determined by the electron drift time from grid to anode.

For the elastic events investigated $t_f \simeq t_{f\ min.} = 2/\mu sec.$

The pulses from the anode were amplified by a pre-amplifier and then switched to an energy channel and an angle channel. Sufficiently large filter constants were used in the energy channel ($\tau_o \simeq 20/\mu sec$) so that the height of the output signal A_E did not

depend on t_f. The amplifier in the angle channel featured differentiation on the delay line and integration with parameters $2\tau_\Lambda = \tau_{int.} = \tau_o$. The τ_o value was selected so that the signal-noise ratio was satisfactory and so that the dependence of the height of the output signal A_Θ on the leading edge t_f was at maximum (Fig. 9). Fig. 14 shows the ratio $A_\Theta / A_E = \psi' \frac{t_f}{\tau_o}$ obtained by calculation for a linearly increasing signal. The angular resolution is determined from the following formula:

$$\frac{\sigma^2(t_f)}{t_f^2} = \frac{\sigma^2(A_E)}{A_E^2} \cdot \frac{\tau_o^2}{t_f^2} \left[\frac{1}{\psi'}\right]^2 \left[\frac{\sigma^2(A_\Theta)}{\sigma^2(A_E)} + \psi^2\left(\frac{t_f}{\tau_o}\right)\right].$$

Here $\sigma^2(A_E)$ and $\sigma^2(A_\Theta)$ are the pulse height resolutions of the energy and angle channels, $\psi' = \partial\psi / \partial\left(\frac{t_f}{\tau_o}\right)$.

An estimate using real parameters gives

$$\frac{\sigma(t_f)}{t_f} \simeq 5 \cdot \frac{\sigma(A_E)}{A_E} \quad \text{or} \quad \sigma(z) \simeq 5 \cdot t_{f\,min.} W \cdot \frac{\sigma(A_E)}{A_E} = 0{,}6\ \text{мм}$$

at $t_{f\ min.} = 2$ μsec, $W = 0.6$ cm/μsec and $\sigma(A_e)/A_E = 0.01$.

Blurring of the track due to electron diffusion also leads to an increase in the leading edge of the pulse at the anode and this may worsen the angular resolution. However, as in the case of the grid transmission effect, a correction may be made according to the drift time measured.

TIME RESOLUTION

The chamber's time resolution is mainly determined by the noise from the pre-amplifier in the cathode channel, by the steepness of rise of the signal and by the characteristics of the shaper. The height of the useful signals at the cathode depends not only on energy

but also on the position of the track in the chamber volume. For a track situated 1 cm from the grid, V_c = 100 keV at T_p = 1.0 MeV. The discriminating threshold must therefore be sufficiently low to ensure high recording efficiency for such events. However, as the threshold is reduced, the number of background processes increases. This number was significantly reduced by means of a special circuit which discriminated background blips in terms of their duration. As a result, the number of errors was less than 1% at a height of V_c = 200 keV and for 40 1/sec. background processes. Fig. 15 shows the matrix of useful events in the co-ordinates recoil proton energy-time window. As is shown in Fig. 15, the time resolution is 0.3 - 0.5 /usec.

DEFINITION OF USEFUL VOLUME

When calculating a differential cross-section, it is important to know the dimensions of the useful volume exactly. Although the cathode-grid distance is known with an accuracy of 0.2%, only part of this volume is actually used. The height of cathode pulses corresponding to tracks situated near the grid is close to zero. For this reason, and also to eliminate background reactions, part of the volume near the grid (~ 2 cm) is not used. Part of the volume close to the cathode (~ 1 cm) is also not used. The position of a track inside the useful volume is determined in terms of $(t_a - t_o)$. Resolution in terms of $(t_a - t_o)$ is mainly determined by fluctuations in the t_a signal, because t_o is emitted by the scintillation counters. The shaper in the energy channel, which determines the instant t_a, features differentiation on the line ($2\tau_\Lambda$ = 3/usec.) and integration (τ_u = 1.5/usec.). The steepness of the useful signal (t_f = 2/usec.) is preserved and noise is reduced to the level of the amplitude channel. The filter's output signal is transmitted to a discriminator which defines the point of maximum steepness and at the same time balances the pulse heights. The time resolution is illustrated in Fig. 16, which shows the time spectrum of the signals $(t_a - t_o)$ for V_a generator pulses varying in height (from 300 keV to 5 MeV). The time resolution is such that the useful volume may be

defined with an accuracy better than 1% assuming that the scale $(t_a - t_o)$ has been calibrated with the same accuracy by linking it to the cathode-grid distance. The calibration was carried out in the following way. The position of the zero on the scale corresponding to tracks in the grid plane was determined using a generator which transmitted pulses at a fixed interval $(t_a - t_o)$. This generator was used to calibrate the linearity of the time analyzer. The second limit, corresponding to tracks in the cathode plane, was determined according to pulses from α-particles. For this purpose, low-energy (2-3 MeV) α-particles were selected whose tracks lay in the cathode plane. The ratio V_c/V_a was measured. The value V_c/V_a depends only on the co-ordinate of the track's centre of mass in the grid-cathode volume and $V_c/V_a = 1$ corresponds to a track lying in the cathode plane. In order to determine $V_c/V_a = 1$, the limit of the α-spectrum (E_α in the range 2-3 MeV) was found, i.e. the maximum value for V_c/V_a. The dependence V_c/V_a on $(t_a - t_o)$ was then plotted for the selected useful events in the energy range 1.2 - 2.5 MeV (in order to exclude fringe effects for V_c and tracks out of parallel with the cathode). The maximum possible value for $(t_a - t_o)$ corresponding to the limit of the volume is obtained by extrapolating this dependence close to a straight line until it intersects with the line $V_c/V_a = 1$. The error for this type of calibration is approximately 2% and this is the main error in defining the useful volume.

ELECTRONICS SYSTEM

The electronics system for the experiment consists of spectrometric channels, a system for the analog selection of events, a counter system, a control system and a system for collecting and storing data. A block diagram of the device and a time diagram of the pulses are shown in Fig. 17 and Fig. 18 respectively.

Signals generated at the chamber's electrodes and amplified by the pre-amplifiers PA are transmitted to the amplifiers A1 - A4 and shapers Sh4 and Sh5. The output signals from the amplifiers and converters C1 and C2 were transmitted to the amplitude storage units.

These units served as an intermediate analog store during the selection of events. Moreover, they standardized the signals for the amplitude-digital code converters.

The trigger signal (event, Fig. 18) is a pulse from the triple coincidence circuit (CC2) which determines the moment when a proton passes through the chamber. The shaper Sh4 shapes a 4 μsec. pulse when a recoil proton is formed. The coincidence (CC3) of this pulse with the trigger signal which passed through the protection and delay unit (PDU3) is the start signal for the event recording system. The protection unit (PDU3) selects an event only if no proton is recorded during the 4 μsec. before or after the event. The control unit (CO-001) shapes the "gate" covering the possible delay range for the signal from the chamber's anode, opens the Sh5 shaper's input and interlocks the shapers in the trigger system Sh1 - Sh3. At the end of the gate, a check is made to see whether there is a test signal from Sh5. If there is a signal, the event recording system is triggered: the output voltage from the pulse height storage units (PHSU 1 - 6) is gated to the amplitude-digital converter system VIST /11/ and as the coding is completed a call is transmitted to the data acquisition system SONIK /12/. If the signal from Sh5 is not received within a given time, the temporary store is discarded and the selection system unlocked. The trigger system is the start signal for the time-amplitude converters C1 and C2 which measure the distribution of events in the time window (C1) and over the chamber volume (C2). The pulses from Sh4 and Sh5 are stop signals. As the Sh4 shaper has a high level of noise activity due to its low threshold, the C2 converter has a start protection circuit (CC3 and distributor D). The event selection circuits are opened by a timer synchronized with the beam in order to avoid any overloading of the system when ejection starts. In order to check the event distribution against the beam duration, the moment when the event occured was recorded in relation to the start of the beam. A linear function voltage generator (LFVG) synchronized with the acceleration cycle was used for this purpose.

As the measurements had to be extremely accurate, it was necessary to use a system whereby a constant check could be kept on the parameters of the counter system, analog selection system and spectrometric system. The monitoring system included a digital precision amplitude generator GAMBIT /13/ and a time interval generator. The voltage from the GAMBIT was proportional to the fixed code N1 (the accuracy of the voltage device was not worse than 10^{-4}) and was transmitted to the precision pulse-height shapers which were connected to the chamber's pre-amplifiers. According to the signals from the precise-time generator (accuracy of time interval - 0.1/usec.), pulses were transmitted to the pre-amplifiers with a polarity and shape similar to those of the chamber's real signals. At the starting instant t_o the photodiodes IS1 - IS3 were fired, simulating the passage of a proton; at that instant the signal reached the cathode, corresponding to the occurence of a recoil proton. At the instant t_{N2} pulses were transmitted to the anode and orifice. The "useful event" in the chamber was thus fully simulated. The channels' stability was checked and their integral non-linearity measured using 16 stages of amplitude for the monitor signals and 8 stages of delay for the signals at the anode (orifice) in relation to the pulse at the cathode. Test events were generated throughout the experiment and the programme for amplitude and time variation was set by means of a special unit. A phasing circuit permitted the generation of a test event only when there was no useful event. By marking the test event, it was possible to identify the test data on the computer. As the test events are a complete simulation of the useful events, it is possible to test the whole system's recording efficiency. The latter was expressed as the ratio of the number of recorded test events to the number counted by the CC4 coincidence circuit. The computer stopped the measurements if efficiency dropped to $< 98\%$.

The counting system consisted of ten scaling circuits connected to a PRINT-OUT console (JINR development). During the experiment the counting system recorded the number of counts from S_1, S_2 and S_3, the number of double coincidences $S_1 \hat{} S_2$, the number of triple coincidences $S_1 \hat{} S_2 \hat{} S_3$, the number of triple coincidences

after the protection unit S_1 S_2 S_3^* (the number of protons recorded), the number of generated pulses recorded by the CC4 circuit and the number of CC3, Sh4 and Sh5 operations. Data from the counting system was fed into the computer via the SONIK system. By comparing the readings from the scaling circuits after each ejection cycle, it was possible to check the efficiency of the counters, the stability of the shapers' thresholds and the efficiency of the event selection system. All the information was fed into a "MINSK-22" computer and was recorded on magnetic tape after the temporary store had been filled. Control matrices and histograms were printed out periodically.

OPERATION ON-LINE WITH COMPUTER

Information from the SONIK system was fed to a "MINSK-22" computer. The restricted capacity of the working store (2 MOZU units each with 4,096 cells; length of one cell - 36 bits) placed very strict demands on the way in which the data were accepted, controlled and recorded on magnetic tape in the peripheral store. Information from SONIK was transmitted to a second MOZU unit; one half of the first unit was set aside as a buffer file. As only 2,048 cells were left for the program, the latter was divided into 2 sections

(1) Acceptance, recording on tape, preparation of control matrices and histograms;
(2) Printing of control matrices and histograms;

which were stored on magnetic tape and automatically switched into the working store when required.

Each event had 4 pulse-height and 3 time co-ordinates. As each co-ordinate is a whole number in the range from 0 to 1,023 , 10 bits are required to record it. In order to deal with information coming from SONIK to the second unit, 4 cells were set aside for each event; the maximum number of events was 1,023. For each event the 12 most significant bits in the first cell were set aside for code. Physical events were represented by zeros in the remaining

24 bits of this cell; generator events were represented by a pulse-height mark (16 possible values - 4 bits) and a time delay mark (8 possible values - 3 bits), and also by an extra unit in 8 bits. Three co-ordinates were recorded in each of the second and third cells and one co-ordinate in the fourth cell. As 70 bits were required to record 7 co-ordinates, each event could be located in two cells (for physical events the remaining two bits were set aside for code; for generator events one bit was set aside for code and 7 bits for pulse height and time delay marks, so that 7 bits were set aside for two of the time co-ordinates). Twice as much information coud thus be recorded on tape and the second unit was kept free for the preparation of control matrices and histograms (the latter were stored on magnetic tape during data acceptance).

After all the fixed bits had been accepted from SONIK and controlled, the data was condensed and sent to the buffer file in the first MOZU unit and then recorded on magnetic tape. The control matrices and histograms were prepared in the second unit. In order to save store space each matrix element was assigned 18 bits; a 64 x 64 matrix was thus located in 2,048 cells. In the case of physical events histograms were prepared for all the co-ordinates (on a scale of 1:16) and also an energy-angle matrix (64 x 64); it was possible to introduce specific thresholds or select "windows" for specific co-ordinates. For generator events histograms were prepared for 5 co-ordinates on a scale of 1:1 (which were printed out as matrices) and for 2 co-ordinates on a scale of 1:16. Moreover, for generator events the average values and variances for each pulse height (or time delay) were calculated. The averaging was done both after a specific length of time and after a whole series of measurements.

Readings from the scaling circuits were periodically fed to the machine. This information was printed out; in addition, efficiency was checked by comparing the readings from the appropriate scaling circuit (CC4) with the number of generator events accepted.

In order to save time when writing the statistics into the program, the following condition was introduced: if the total number of events accepted was less than 1,023 (when one of the scaling circuits was overloaded, data taking at the SONIK was stopped and the information and scaling circuit readings already acquired were sent to the computer), the data were only condensed and transferred to the buffer file in the first unit, after which the scaling circuit readings were taken. It was only then (at the same time as fresh data were acquired from SONIK) that the remaining operations requiring the largest amount of time were performed; access to the peripheral store and preparation of matrices and histograms.

When the information was recorded on magnetic tape, a check reading was carried out by comparing the check sums. When there was a clash, the corresponding area was omitted. In order to facilitate reading during processing and to ensure reliability, the check sums for the recorded files were reduced to "standard" form (units in all bits). The program was written in the algorithmic language "AKI" using machine language. A block diagram of the program is shown in Fig. 19.

MEASUREMENT OF THE DIFFERENTIAL CROSS-SECTION OF pp SCATTERING AT 1000 MeV

The experiment at a proton energy of 1000 MeV was mainly carried out in order to check the method as the existing experimental data were in agreement with each other and did not contradict the theory of dispersion relations.

The layout of the experiment is shown in Fig. 20. The intensity of the extracted beam extended in time was $\sim 10^4$ protons/sec. at a $\sim$ 60% duty cycle. The rate of acquisition of useful events was $\sim$ 120 pulses/hour. Altogether approximately 3000 useful events were recorded.

The stability of the device and the event recording efficiency were continuously checked during the measurements. Pulses from α -particles (E_α = 4.76 MeV) used for calibration were simultaneously recorded. The measurement was carried out during one cycle without re-filling the chamber. There was no noticeable difference in the α -spectra obtained with the beam and without the beam. The processing of the experimental data mainly comprised the deduction of the background and the definition of the effective useful volume. The background value (reactions at the chamber's electrodes, scattering of neutrons on hydrogen et al.) increases as the recoil proton energy decreases. The minimum energy of the recoil protons used for processing was $\sim$ 1.25 MeV, and the value of the background deducted did not exceed 20% of the number of events. At higher T_p energies the ratio of background to useful events drops rapidly and at 3 MeV the background does not exceed 1%. In order to attain the region of lowest momentum transfer, it is necessary to use a more sophisticated trigger system, for example proportional chambers.

The background was deducted in the following way: Events were selected in terms of angle in the energy-angle matrix (Fig. 21). In order to take into account the contribution by the neutron background in the energy-time window matrix (Fig. 15), the pedestal of random coincidences was deducted from the event peak for each energy. In the recoil proton energy range from 3 to 4 MeV, the combined anode+ orifice pulses are used for this operation (1.4% of the combined pulse height caused by the mutual inductances is deducted). The background is negligible at these energies.

Fig. 22 shows the dependence of the difference cross-section $d\sigma/dT_p$ on the recoil proton energy. By using the interference formula the parameters α = -0.10 $\pm$ 0.08 and β = 0.01 $\pm$ 0.06 were determined. These results are in good agreement both with the theoretical values /14, 15/ and the experimental data previously obtained /16, 17/ by another method.

POSSIBLE DEVELOPMENTS OF THE METHOD

The method's capabilities for investigating elastic pp scattering at E_p = 1000 MeV were illustrated above. The method could be improved further by using proportional chambers to trigger the ionization chamber. In this case the trigger pulse would be generated only if the particle entering the chamber was scattered at an angle greater than $\Theta_{min.}$ According to calculations, the number of triggered pulses will be $\sim 1\%$ of the number of particles passing through. In the same way the background of random coincidences will be reduced 100 times. This will allow beam intensity to be boosted to $\sim 10^5$ particles/sec. and, consequently, the data acquisition rate will be increased by an order of magnitude. A further increase in the counting rate may be achieved by increasing the number of chamber modules located in 1 volume (for example, up to 6 modules). In addition, by using proportional chambers the primary particle's scattering angle Θ may be recorded, and the correlation $\Theta - T_p$ will serve as an additional criterion for selecting elastic events. An improved chamber of this type may be used to study scattering of various high-energy particles ($\pi^{\pm}$, $K^{\pm}$, n, $\bar{p}$, etc.) on hydrogen. Moreover, the possibility of using other gases such as deuterium and helium is an interesting prospect.

The authors are very grateful to their colleagues in the design office, development shop, low-temperature physics department, radio-chemistry laboratory and the LFVE radio-electronics department for designing and manufacturing the chamber, for carrying out the vacuum tests, for providing the pure hydrogen, for performing the gas analysis and for preparing the apparatus. The authors are also very grateful to their colleagues in the accelerator department, who ran the synchro-cyclotron in the "pseudo-stretch" mode. The authors also wish to thank M.F. Sobolevskij for his help in processing the measurement results.

---ooOoo---

Bibliography

1. G. Bellettini et al. Phys. Lett., 19, 705 (1966).
2. K.J. Foley et al. Phys. Rev. Lett., 19, 857 (1967).
3. G.G. Vorob'ev et al. JINR Preprint EI-4445, Dubna, 1969.
4. V.A. Nikitin. Proceedings of the fifth Winter School on nuclear theory and high-energy physics, part II, p. 41, 1970.
5. A.A. Vorob'ev, V.A. Korolev. PTE, N° 4, 42 (1961).
6. J.S. Townsend, V.A. Bailey. Phil. Mag., 42, 873 (1921).
7. U. Fano. Phys. Rev., 72, 26 (1947).
8. A.A. Vorob'ev, V.A. Korolev. PTE, N° 2, 78 (1961).
9. Eksperimental'naya yadernaya fisika. Red. E. Segre, Vol. I, p. 200, Publ. house In. Lit. 1955.
10. Eksperimental'naya yadernaya fisika. Red. E. Segre, Vol. I, p. 166, Publ. house In. Lit. 1955.
11. V.I. Kadashevich, V.I. Vinogradov. V.V. Marchenkov, A.P. Nekhaj. Preprint FTI-199, Leningrad 1969.
12. I.I. Tkach, A.V. Kulikov, A.P. Kashchuk, N.K. Lastochkin, S.I. Kalentarova, G.A. Gorodnitskij. Preprint FTI-185, Leningrad 1969.
13. N.K. Lastochkin, V.N. Inzhevatov, E.E. Yakovlev. PTE, 1, 109 (1971).
14. V.S. Barashenkov, V.D. Toneev. Preprint JINR P2-3850, Dubna (1968).
15. O.V. Dumbrajs. Ya. F., 5, 1096 (1971).
16. J.D. Dowell, K.J. Homer, Q.H. Khan, W.K. McFarlane, J.S.C. McKee, A.W. O'Dell. Phys. Lett., 12, 252 (1964).
17. L.M.C. Dutton, R.J.W. Howells, J.D. Jafar, H.B. van der Raay. Phys. Lett., 25B, 245 (1967).

---ooOoo---

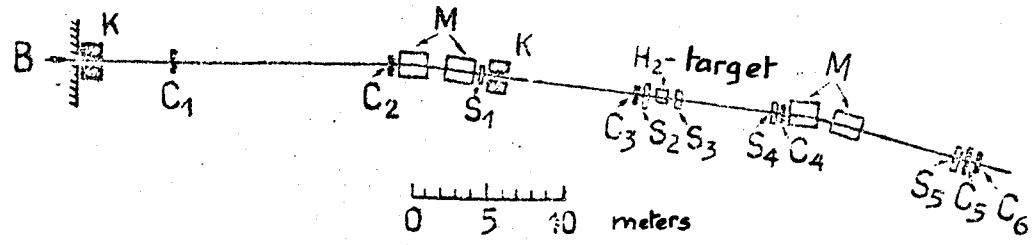

Fig. 2. Experimental layout used to measure small-angle scattering cross-section by recording the scattering angle.

B - beam, K - collimators,
M - sweeping magnets,
C - scintillation counters,
S - spark chambers.

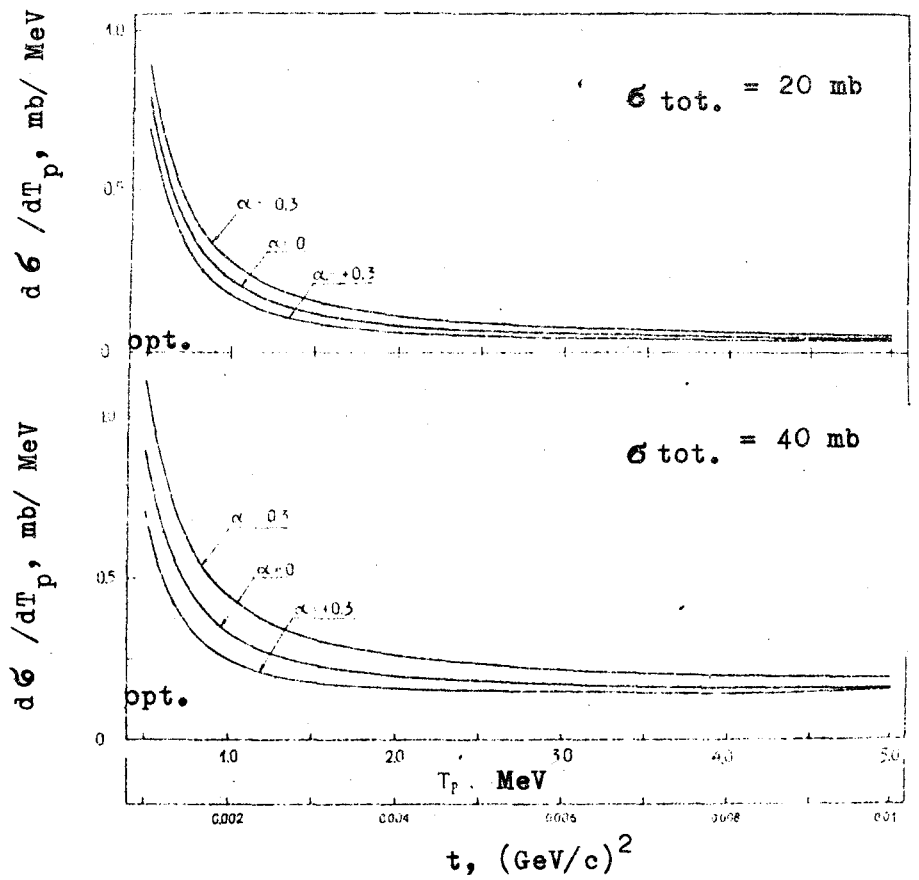

Fig. 1. Differential cross-sections of hadron elastic scattering at small angles at various total cross-section values.

$$\alpha = \frac{\mathrm{Re}\, A_{ns}(0)}{\mathrm{Im}\, A_{ns}(0)}$$

The figure shows the "optical" point corresponding to the cross-section

$$\left(\frac{d\sigma}{dT_p}\right)_{opt.} = \frac{M \cdot \sigma^2_{tot.}}{8\pi}, \quad \hbar = c = 1.$$

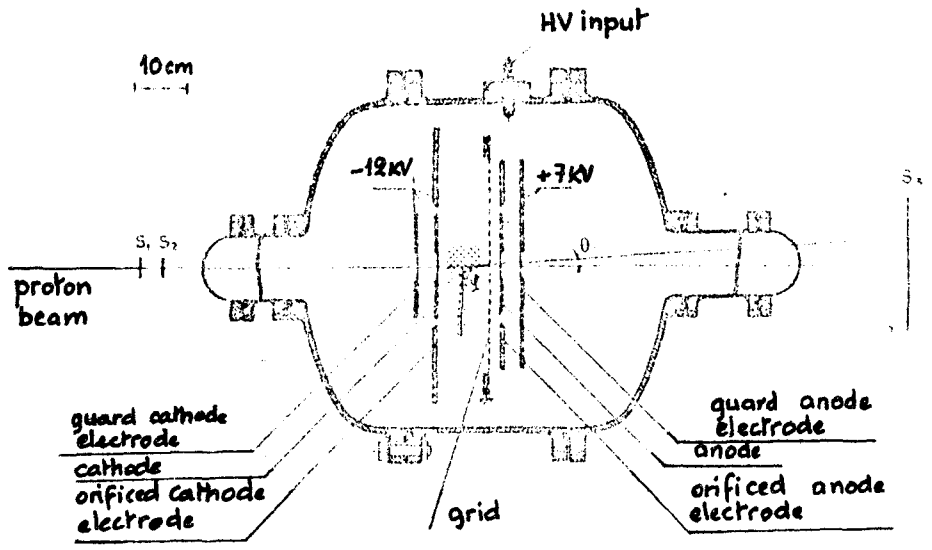

Fig. 3. Pulsed ionization chamber used to record recoil protons.

Diameter of central electrodes 200 mm, internal diameter of orifice 220 mm, external diameter of orifice 400 mm, cathode-grid distance 100.0 $\pm$ 0.2 mm.

$S_1 S_2 S_3$ - control telescope of scintillation counters.

Hydrogen pressure in the chamber 8 atm.

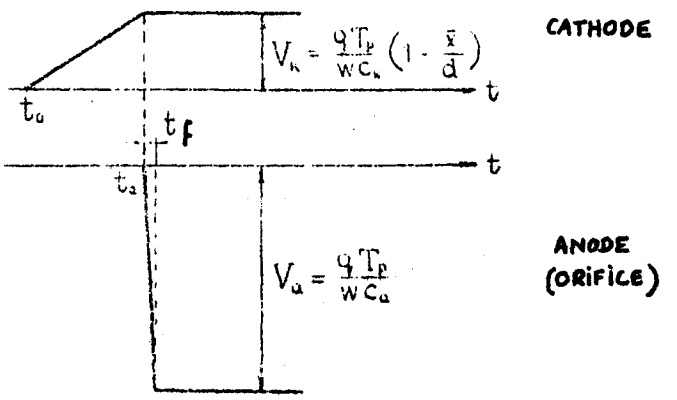

Fig. 4. Pulses occuring at the chamber electrodes.

V_c - pulse height at cathode,

V_a - pulse height at anode,

q - electron charge,

T_p - recoil proton energy,

W - average production energy of ion pairs,

C_c - cathode-earth capacitance,

C_a - anode-earth capacitance,

d - cathode-grid distance,

$\bar{x}$ - distance from ions' centre of gravity to cathode,

t_o - instant at which scattering took place,

t_a - instant at which pulse occured at anode,

t_f - leading edge of pulse at anode.

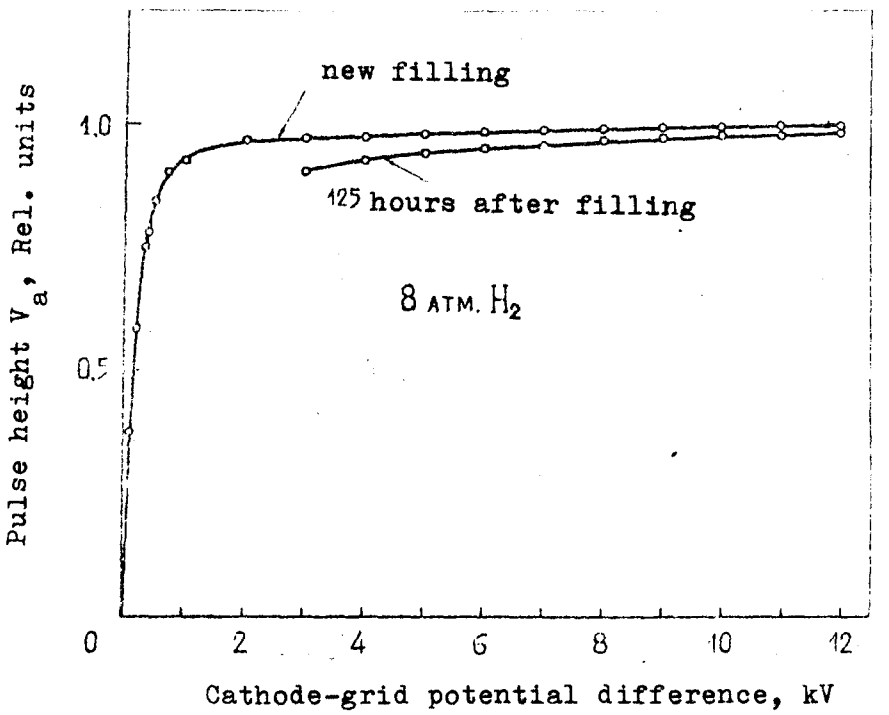

Fig. 5. Dependence of anode pulse heights on electric field value.

Cathode-grid distance 100 mm.

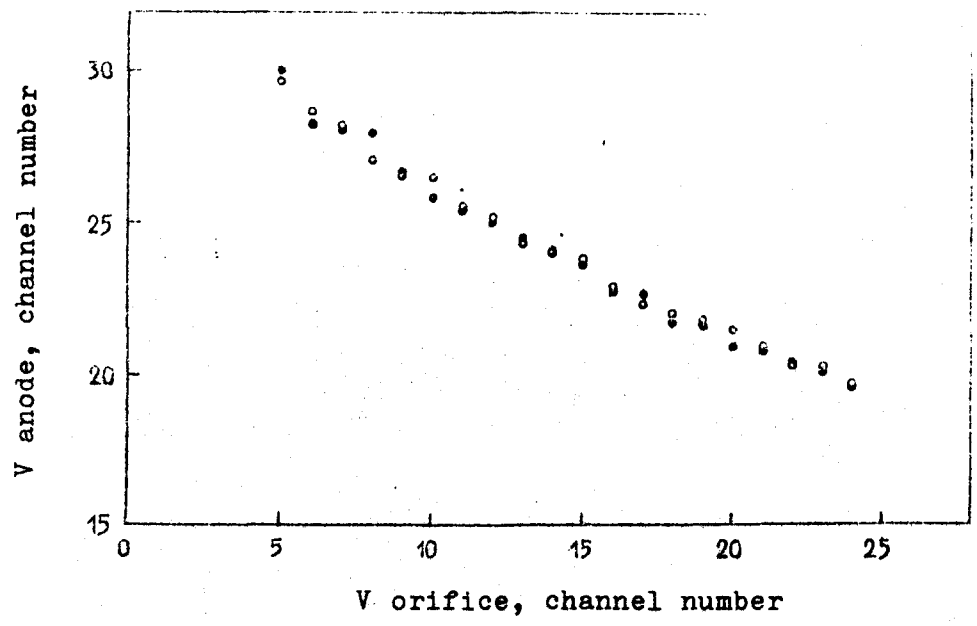

Fig. 6. Positions of distributions peaks of anode pulse heights at fixed orifice pulse heights.

o - distribution peaks of pulses corresponding to recoil protons produced in the half of the chamber's useful volume nearest the cathode.

• - the same for recoil protons produced in the half of the chamber's useful volume nearest the grid.

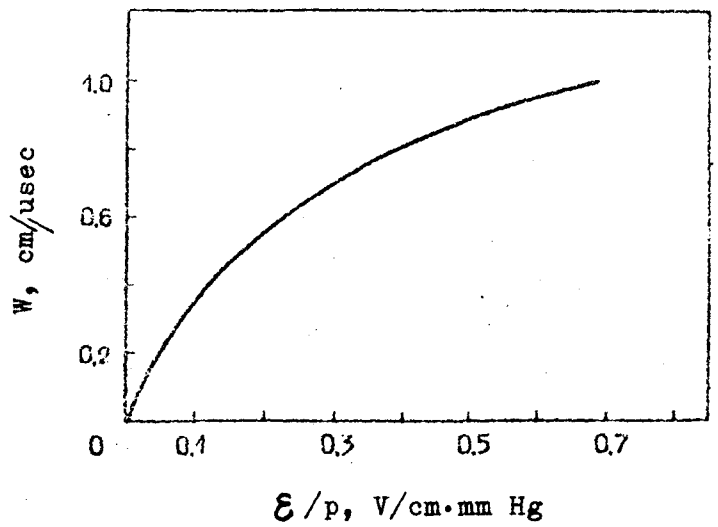

Fig. 7. Dependence of electron drift rate in hydrogen on electric field value.

ε - electric field strength,
p - hydrogen pressure.

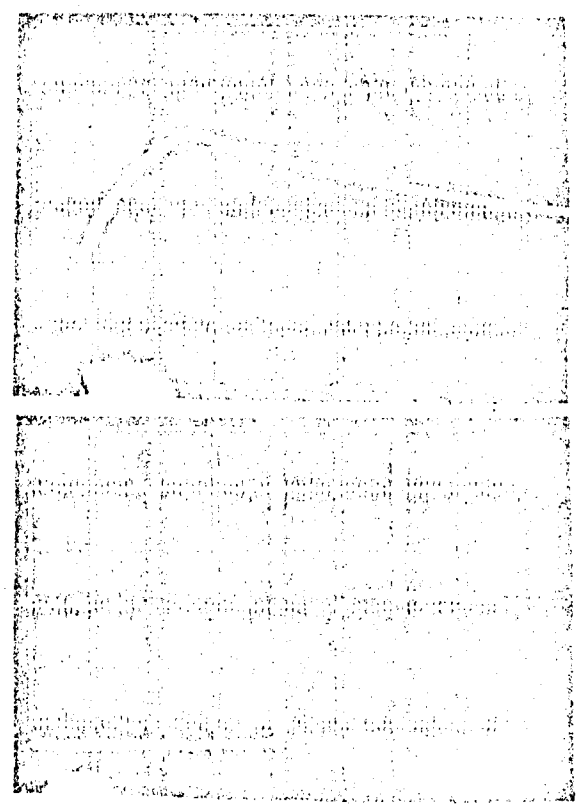

a)

b)

Fig. 8. Photographs of α-particle pulses at the chamber electrodes (after pre-amplifiers).

a) pulse at cathode.
1 division = 10 /usec.

Slow pulse decay is caused by differentiation in th amplifier.

b) pulse at anode.
1 division = 2 /usec.

The pulse corresponds to an α-particle emerging almost in parallel to the cathode surface. The sharp beginning and end of the pulse indicate that track blur caused by diffusion is not great.

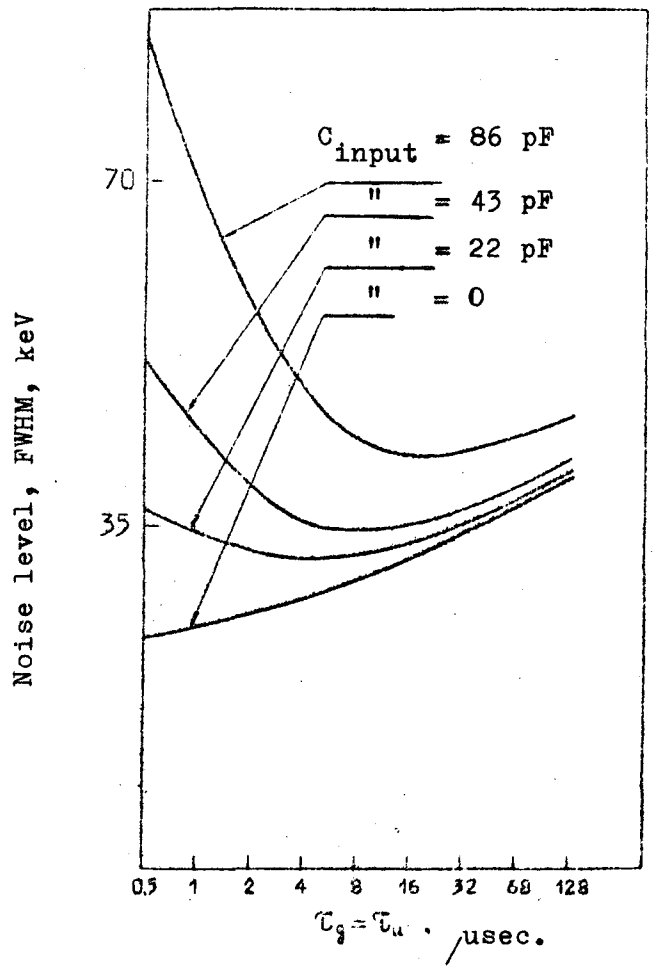

Fig. 9. Dependence of pre-amplifier noise level on pass band at various input capacitances.

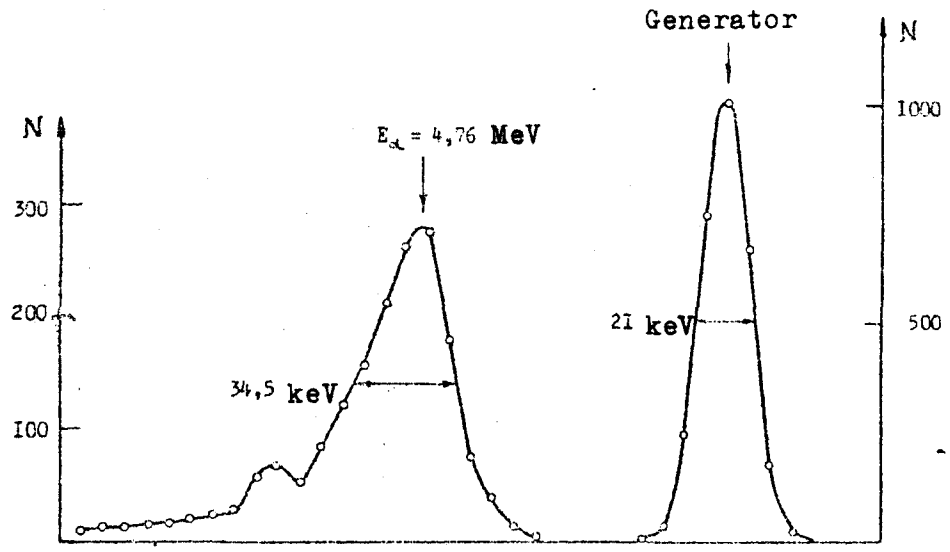

Fig. 10. ^{234}U α-spectrum measured on a dummy hydrogen ionization chamber.

A very low noise level was achieved during these measurements.

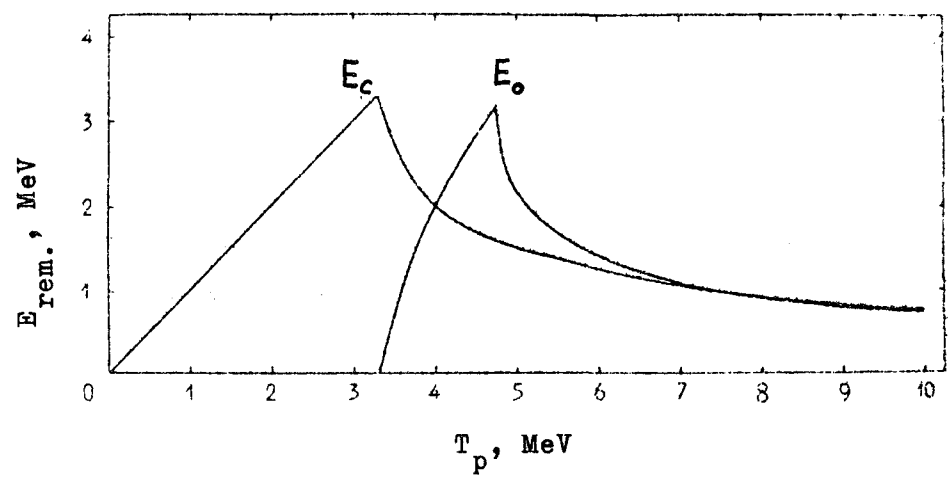

Fig. 11. Dependence on proton energy T_p of the energy left by a proton in the volume defined by the central anode E_c and orifice E_o. It is assumed that the proton emerges from the centre of the chamber in parallel to the electrode. The calculation was done using the path-energy dependence.

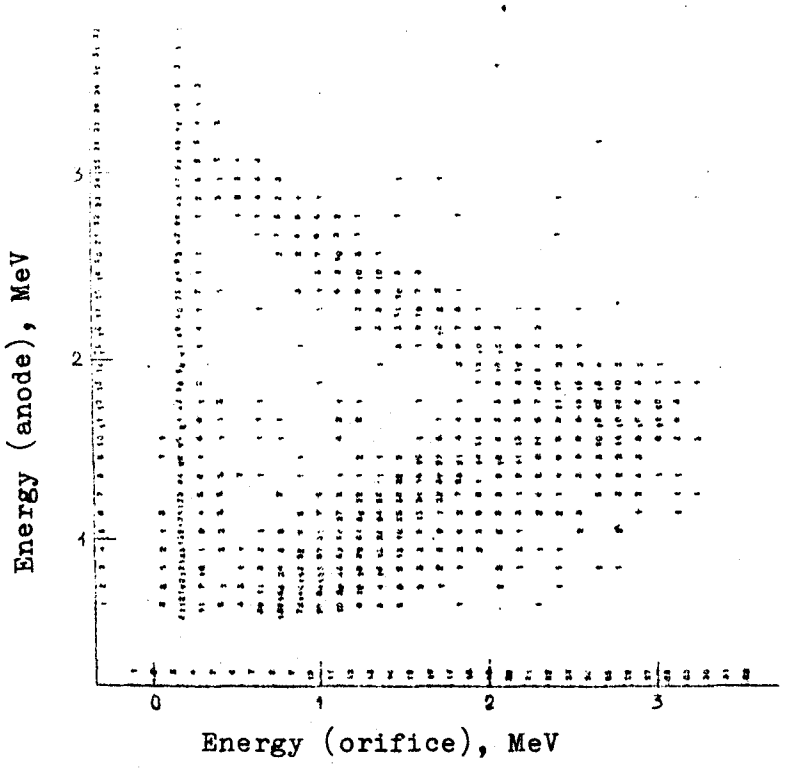

Fig. 12. Matrix of elastic events in the co-ordinates anode pulse height-orifice pulse height. The measurements were carried out at $P_{lab.}$ = 1.34 GeV/c.

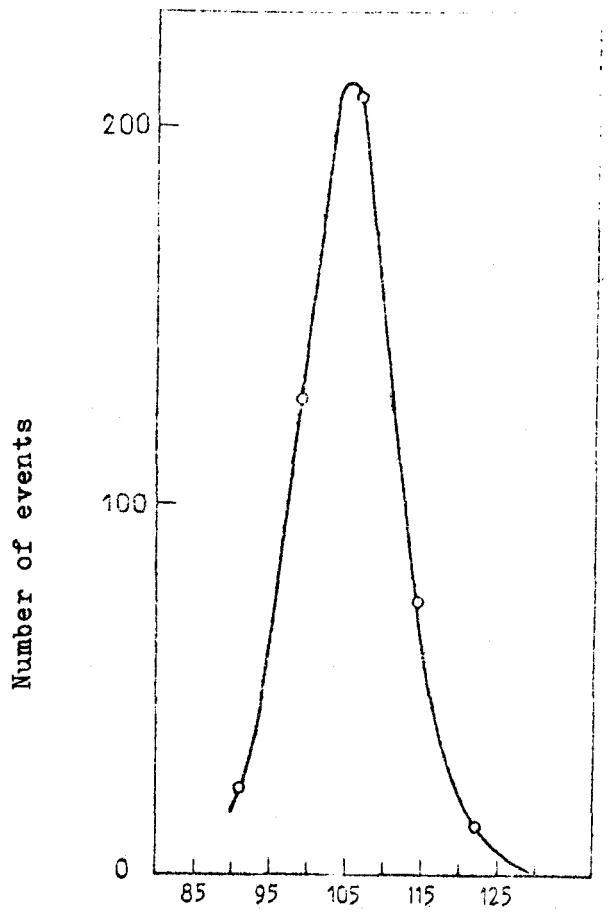

Fig. 13. Distribution of recoil protons according to path at a fixed orifice pulse height. The distribution was plotted using the path-energy dependence, and the recoil proton energy was determined by linear calibration of the energy scale in relation to the α-particle momenta. The coincidence of the distribution centre with the anode radius confirms that the energy calibration is correct.

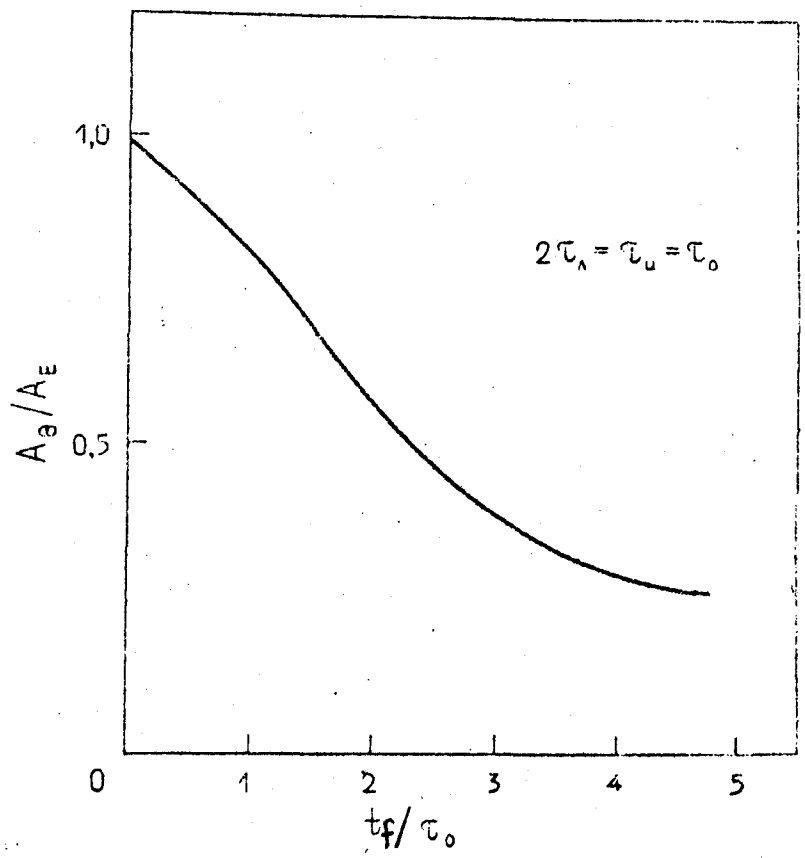

Fig. 14. Dependence of the pulse heights in the angle and energy channels on the pass band of the amplifier in the angular channel. The calculation was made for linearly increasing signals with leading edge t_f.

τ_A - time constant of differentiating line,

τ_u - time constant of integration.

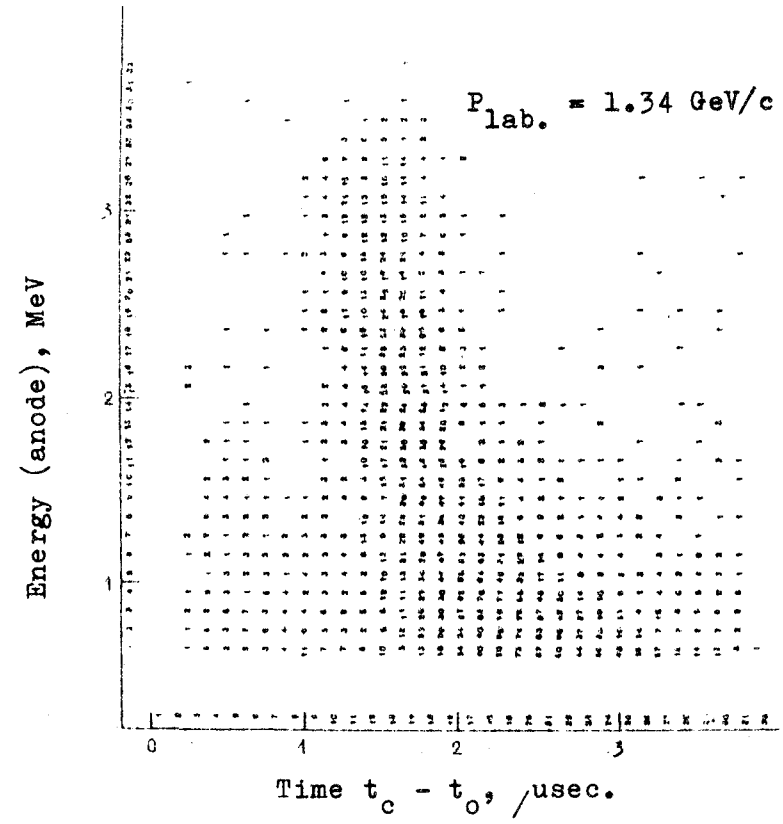

Fig. 15. Distribution of events in time window.

t_o - instant of traversal of proton,

t_c - instant at which pulse occurs at cathode.

The measurements were carried out at $P_{lab.}$ = 1.34 GeV/c.

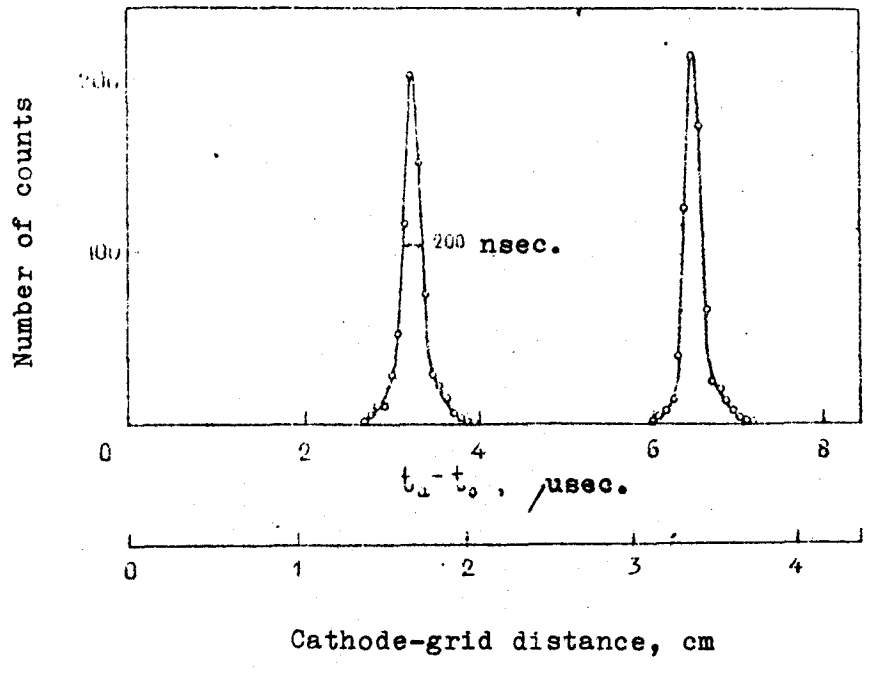

Fig. 16. Time spectrum of generator signals with fixed interval $t_a - t_o$.
The signal height V_a varied from 300 keV to 5 MeV during the measurements.
The scale underneath defines the method's spatial resolution.

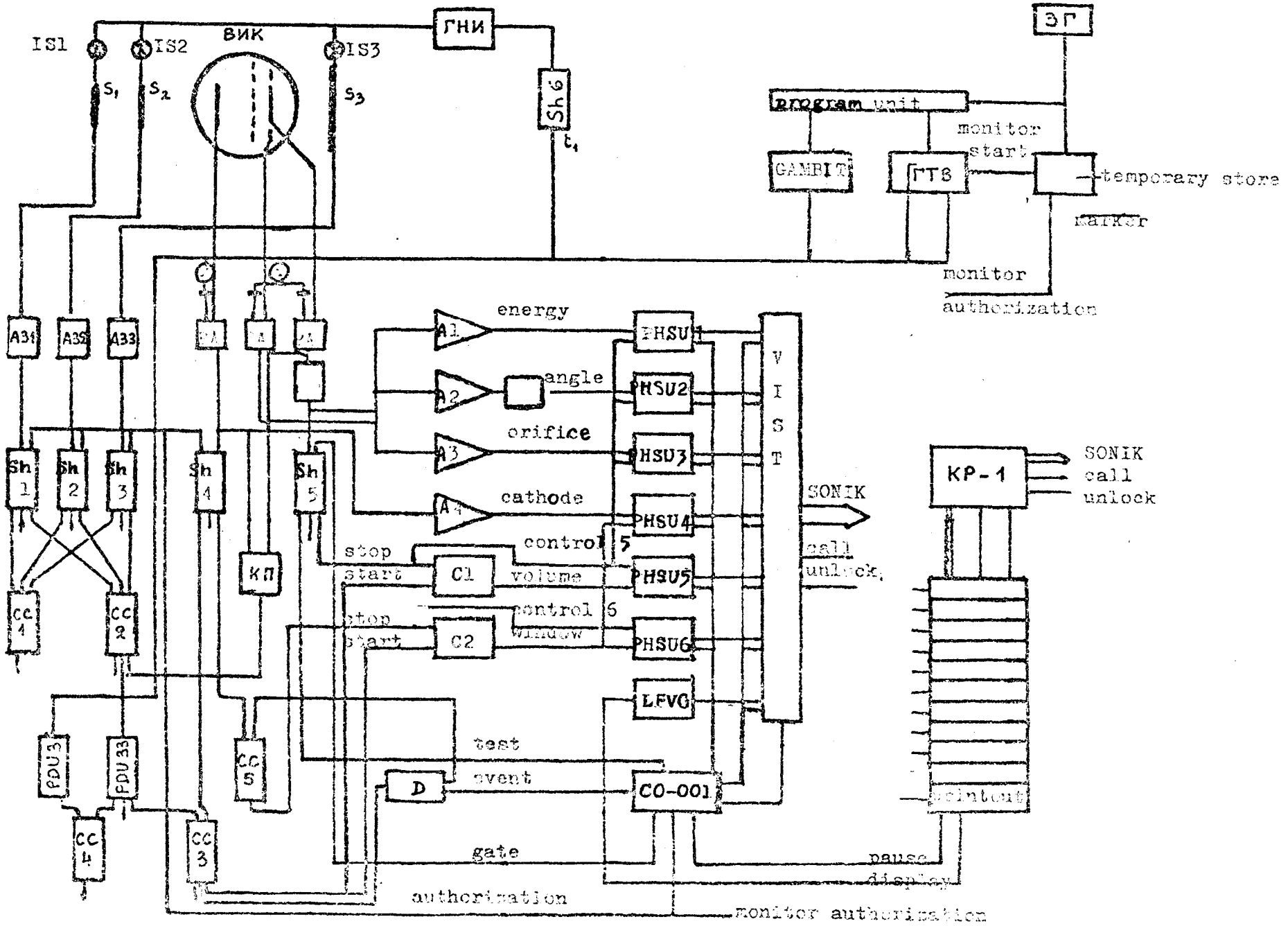

Fig. 17. Block diagram of electronics circuit.

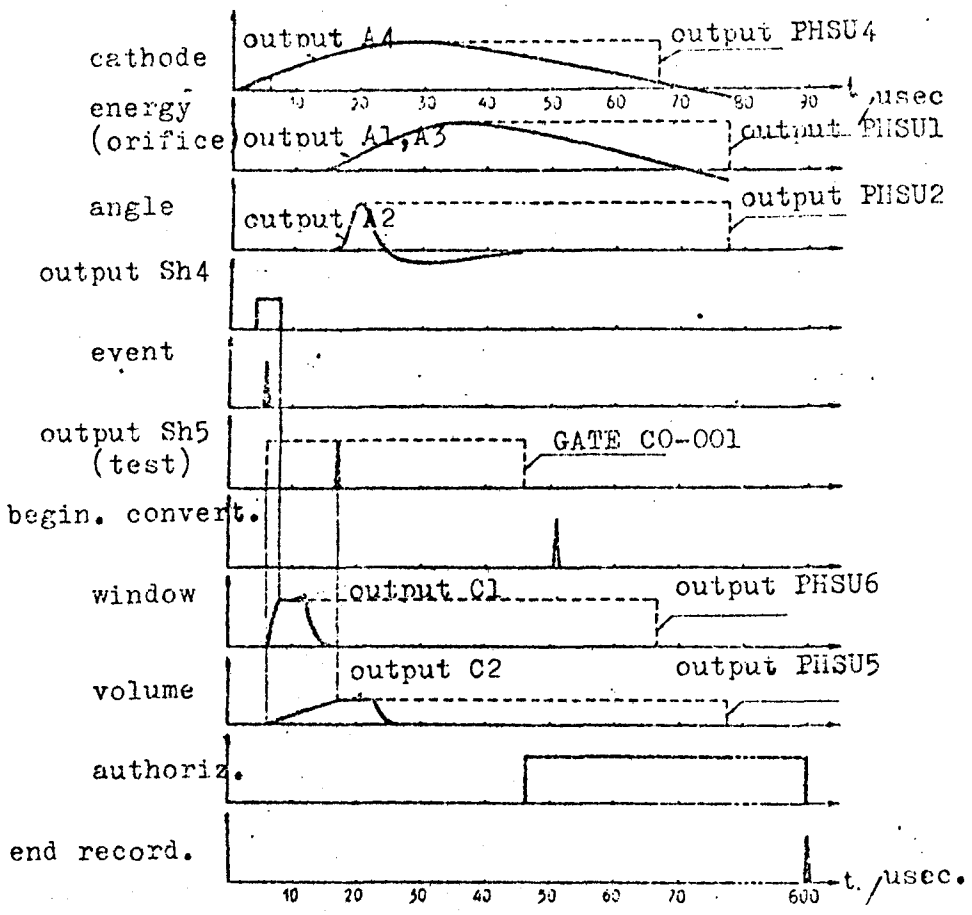

Fig. 18. Time diagram of pulses.

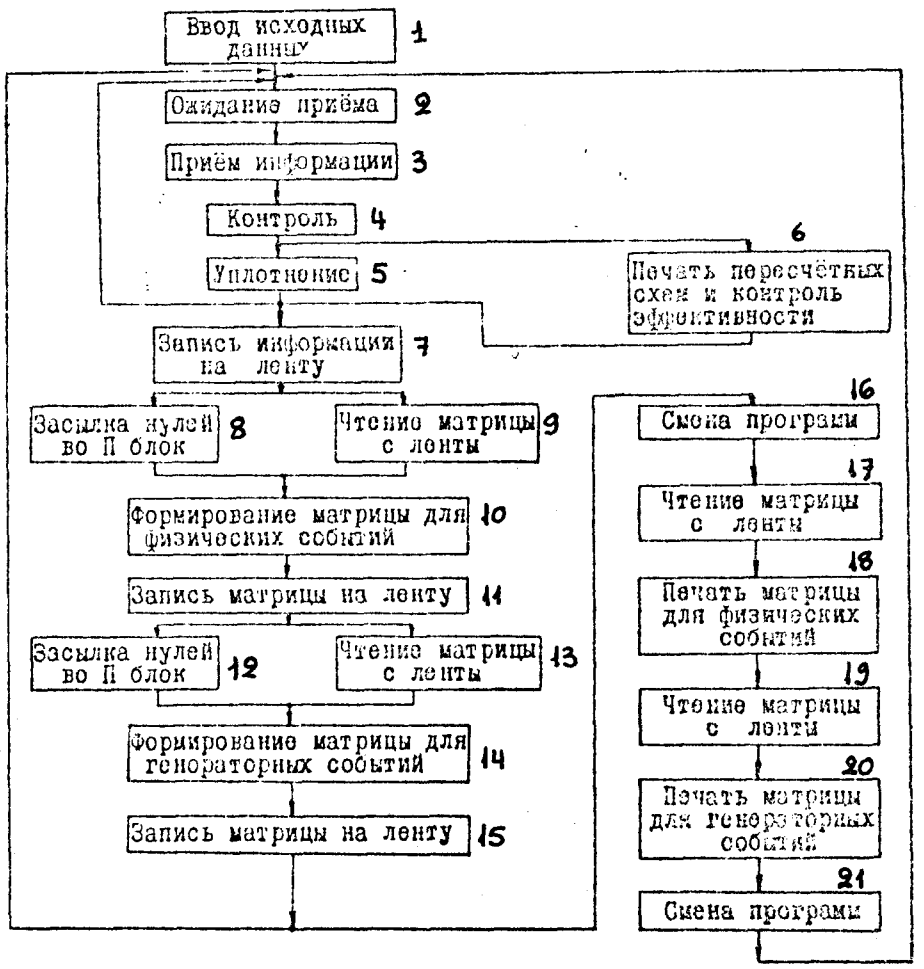

Fig. 19. Block diagram of computer program.

1. Data input
2. Await acceptance
3. Accept data
4. Control
5. Condensation
6. Scaling circuits' print-out and efficiency check
7. Record data on tape
8. Send zeros to unit II
9. Read matrices from tape
10. Prepara matrices for physical events
11. Record matrices on tape
12. Send zeros to unit II
13. Read matrices from tape
14. Prepare matrices for generator events
15. Record matrices on tape
16. Change program
17. Read matrices from tape
18. Print matrices for physical events
19. Read matrices from tape
20. Print matrices for generator events
21. Change program

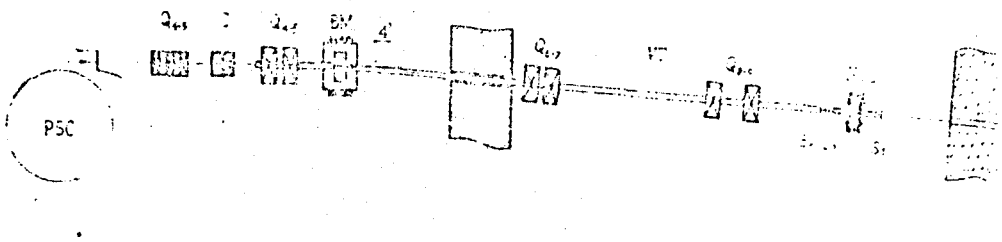

Fig. 20. Layout of experiment to measure $d\sigma_{pp}/dt$ at a proton energy of 1000 MeV.

PSC - proton synchrocyclotron

Q_{1-9} - quadrupole magnet lenses

C - collimator with adjustable slit

BM - bending magnet

VT - vacuum channel

HIC - hydrogen ionization chamber

$S_1S_2S_3$ - telescope of scintillation counters

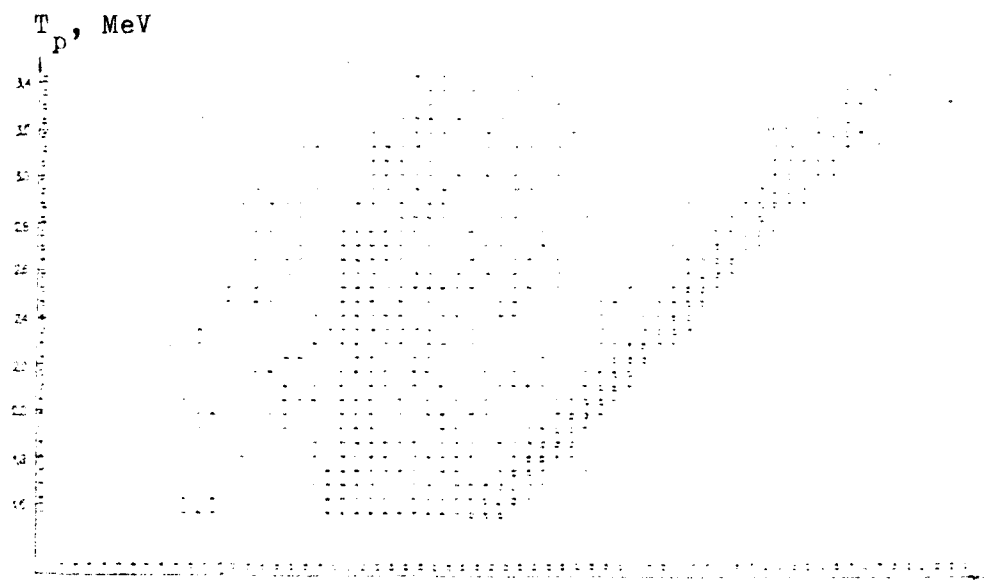

Fig. 21. Matrix of events in energy-pulse height coordinates in angular channel. Elastic events are grouped near the diagonal. The background on the left is caused by nuclear reactions and scattering of neutrons on hydrogen.

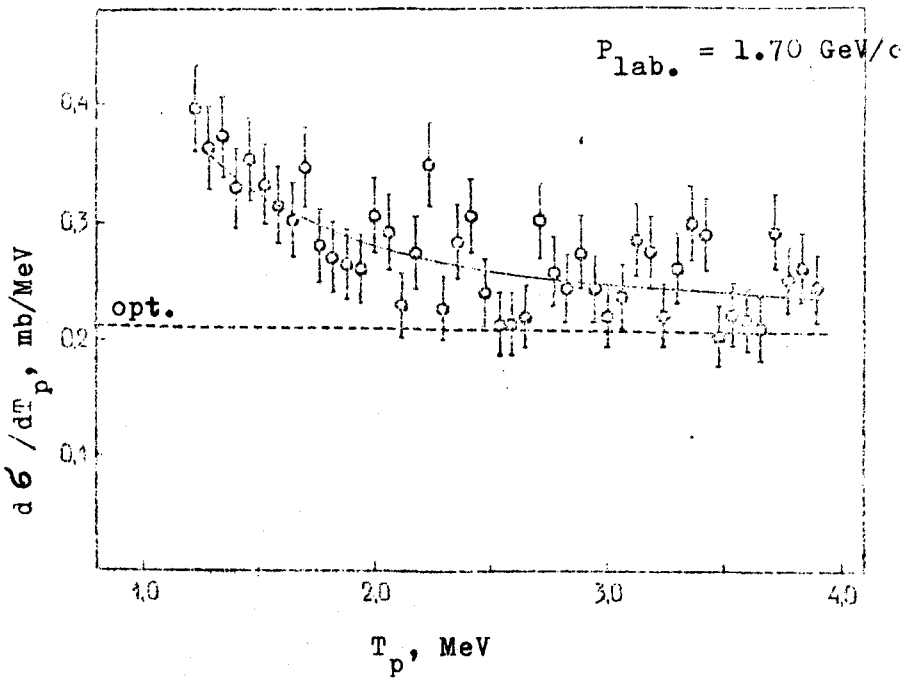

Fig. 22. Differential cross-section of elastic pp scattering at $P_{lab.}$ = 1.7 GeV/c.
The solid line indicates the result obtained by the interference formula

$$\frac{d\sigma}{dT_p} = \left(\frac{d\sigma}{dT_p}\right)_{opt.} \left[1 + \beta + \left(\alpha - \frac{A_c}{Im\, A_{ns}(0)}\right)^2\right] \cdot \exp\left(-A|t|\right),$$

where $\alpha = \frac{Re\, A_{ns}(0)}{Im\, A_{ns}(0)}$, $\left(\frac{d\sigma}{dT_p}\right)_{opt.} = \frac{M \cdot \sigma^2_{tot.}}{8\pi}$,

$A_c = \frac{2}{137 \cdot M \cdot T_p \cdot \beta_p}$ - is the Coulomb amplitude,

$Im\, A_{ns}(0) = \frac{k}{4\pi} \cdot \sigma_{tot.}$; M is the nucleon's mass,

$\sigma_{tot.}$ is the total cross-section of the pp interaction, β is the parameter allowing for the contribution by spin-independent amplitudes, $A = 5\ (GeV/c)^{-2}$, $\hbar = c = 1$, k and β_p are the momentum and velocity of the incident proton. The dotted line is $\left(\frac{d\sigma}{dT_p}\right)_{opt.} \cdot \exp\left(-A|t|\right)$.

The parameters α and β were determined by the least squares method.